

Microscopic two-nucleon overlaps and knockout reactions from ^{12}C

E. C. Simpson,¹ P. Navrátil,² R. Roth,³ and J. A. Tostevin^{1,4}

¹*Department of Physics, Faculty of Engineering and Physical Sciences, University of Surrey, Guildford, Surrey GU2 7XH, United Kingdom*

²*TRIUMF, 4004 Wesbrook Mall, Vancouver, British Columbia V6T2A3, Canada*

³*Institut für Kernphysik, Technische Universität Darmstadt, 64289 Darmstadt, Germany*

⁴*National Superconducting Cyclotron Laboratory, Michigan State University, East Lansing, Michigan 48824, USA*

(Received 20 July 2012; revised manuscript received 18 October 2012; published 29 November 2012)

The nuclear structure dependence of direct reactions that remove a pair of like or unlike nucleons from a fast ^{12}C projectile beam are considered. Specifically, we study the differences in the two-nucleon correlations present and the predicted removal cross sections when using p -shell shell-model and multi- $\hbar\omega$ no-core shell-model (NCSM) descriptions of the two-nucleon overlaps for the transitions to the mass $A = 10$ projectile residues. The NCSM calculations use modern chiral two-nucleon and three-nucleon (NN + 3N) interactions. The np -removal cross sections to low-lying $T = 0$, ^{10}B final states are enhanced when using the NCSM two-nucleon amplitudes. The calculated absolute and relative partial cross sections to the low-energy ^{10}B final states show a significant sensitivity to the interactions used, suggesting that assessments of the overlap functions for these transitions and confirmations of their structure could be made using final-state-exclusive measurements of the np -removal cross sections and the associated momentum distributions of the forward traveling projectile-like residues.

DOI: [10.1103/PhysRevC.86.054609](https://doi.org/10.1103/PhysRevC.86.054609)

PACS number(s): 24.50.+g, 25.70.Mn, 21.10.Pc

I. INTRODUCTION

Properties of the wave functions of pairs of nucleons in a mass $A + 2$ projectile can be probed using sudden two-nucleon removal reactions that exploit fast, surface-grazing collisions of the projectile with a light target nucleus. The sensitivity is to the wave functions of the nucleons at and near the surface of the projectile. When combined with γ -decay spectroscopy, partial cross sections of populated final states in the mass A reaction residues can be determined. This direct reaction mechanism, its cross sections, and their distributions with the momenta of the forward traveling residues are now being exploited as a spectroscopic tool in studies of the evolution of nucleon single-particle structure near the Fermi surfaces of some of the most exotic nuclei; see, for example, Refs. [1–3] and citations therein. The reaction observables used are, currently, inclusive with respect to the final states of both the removed nucleons and the struck light target nucleus. More exclusive measurements, e.g., of the light charged fragments in the final state, may in the future provide additional probes of the projectile structure [4].

A detailed discussion of the two-nucleon removal reaction mechanism, its eikonal reaction-dynamical description, and the cross sections and their momentum distributions, in the case of high-energy two-nucleon removal from ^{12}C , was presented in Ref. [5]. A feature of this model description is that the removal cross sections involve only elastic interactions of the projectile residues with the target but sums of contributions from both elastic and inelastic interactions of one or both nucleons with the target [6]. New data, for the sd -shell nucleus ^{28}Mg and the $^{28}\text{Mg}(-2p)$ reaction, have quantified these different contributions experimentally [7] and have confirmed that the relative importance of these different processes to the cross sections are consistent with the predictions of the eikonal dynamical model. This has provided an important additional test of the reaction model. In the earlier work for ^{12}C [5], the theoretical comparisons used the sums of

these removal contributions and p -shell ($0\hbar\omega$ shell-model) structure calculations were used to construct the required $\langle^{10}\text{X}(J_f^\pi, T)|^{12}\text{C}\rangle$ two-nucleon overlaps. The WBP [8] and P1T [9] shell-model effective-interaction Hamiltonians were used.

Several key elements of that analysis are also relevant here:

(i) The reaction is geometrically selective [10] and the two-nucleon removal cross sections will be enhanced if the projectile ground state has components with pairs of nucleons with strong spatial correlations (localization).

(ii) The available experimental cross section data, from high-energy primary-beam measurements, are inclusive with respect to the populated bound states of the residues following np , nn , and pp removal [11,12]. The data, at three energies, reveal a significant enhancement of the ratio of unlike-pair yields, σ_{-np} , to those for the like-nucleon pairs, σ_{-nn} and σ_{-pp} . This enhancement is significantly greater than that expected based simply on the numbers of available two-nucleon-pair combinations (i.e., a factor of 8/3). For example, the experimental $\sigma_{-np}:\sigma_{-nn}$ ratio was 8.54 for the data set with a ^{12}C beam with an energy of 2.1 GeV per nucleon. Some (but not all) of this enhancement could be explained as due to the pair correlations already generated in $0\hbar\omega p$ -shell-model overlap functions and because a larger fraction of the nn -removal strength leads to unbound ^{10}C final states. However, the experimental σ_{-np} values remained factors of 1.45 to 2.2 larger than the theoretical model calculations for the three available data sets [11,12]. Table I, reproduced from Ref. [5], shows both the p -shell-model results and data.

(iii) The shapes and widths of the reaction residues' momentum distributions have both diagnostic and spectroscopic value, being indicative of the total angular momentum I , the total orbital angular momentum L , and hence, with $(LS)I$ coupling, also the total spin S carried by the removed nucleon pair [13].

(iv) The calculated cross sections for the $T = 1$ states common to all three residues, namely, the first 0^+ and 2^+ states,

TABLE I. Calculated and experimental cross sections for two-nucleon removals from ^{12}C , for projectile energies of 250, 1050, and 2100 MeV per nucleon, from [5]. All cross sections are in millibarns. The calculations use p -shell shell-model wave functions from the WBP effective interaction.

Energy (MeV/u)	^{10}Be			^{10}C			^{10}B		
	σ_{-2N}	σ_{exp}	$\sigma_{\text{exp}}/\sigma_{-2N}$	σ_{-2N}	σ_{exp}	$\sigma_{\text{exp}}/\sigma_{-2N}$	σ_{-2N}	σ_{exp}	$\sigma_{\text{exp}}/\sigma_{-2N}$
250 [11]	7.48	5.88 ± 9.70	0.79 ± 1.30	5.80	5.33 ± 0.81	0.92 ± 0.14	21.57	47.50 ± 2.42	2.20 ± 0.11
1050 [12]	6.62	5.30 ± 0.30	0.80 ± 0.05	5.13	4.44 ± 0.24	0.87 ± 0.05	19.27	27.90 ± 2.20	1.45 ± 0.11
2100 [12]	6.52	5.81 ± 0.29	0.89 ± 0.04	5.04	4.11 ± 0.22	0.82 ± 0.04	19.02	35.10 ± 3.40	1.84 ± 0.18

are essentially equal. Minor differences in the calculations arise from the small differences in the empirical separation energies for each system. Unlike the np -removal case, these calculated inclusive $T = 1$ cross sections were reasonably consistent with and were fractionally larger than the data values for σ_{-nn} and σ_{-pp} , suggesting that the deficit in the theoretical cross sections in the np channel reflects, primarily, a failure of our description of the overlaps $\langle ^{10}\text{B}(J_f^{\pi}, T = 0) | ^{12}\text{C} \rangle$ for the transitions to the $T = 0$, ^{10}B final states.

We exploit the eikonal reaction model in the isospin formalism [6,10,14] for the removal of the like ($T = 1$) and unlike ($T = 0, 1$) pairs of nucleons from ^{12}C . In particular, we will investigate the effect on reaction observables when using *ab initio* multi- $\hbar\omega$ no-core shell-model (NCSM) descriptions for the two-nucleon overlaps. We contrast these with the earlier $0\hbar\omega$ p -shell shell-model results of Ref. [5].

Here we will discuss only the np - and nn -removal channels, to ^{10}B and ^{10}C . These two channels share the same two $T = 1$ final configurations, the 0_1^+ and 2_1^+ states (see, e.g., Fig. 1), and

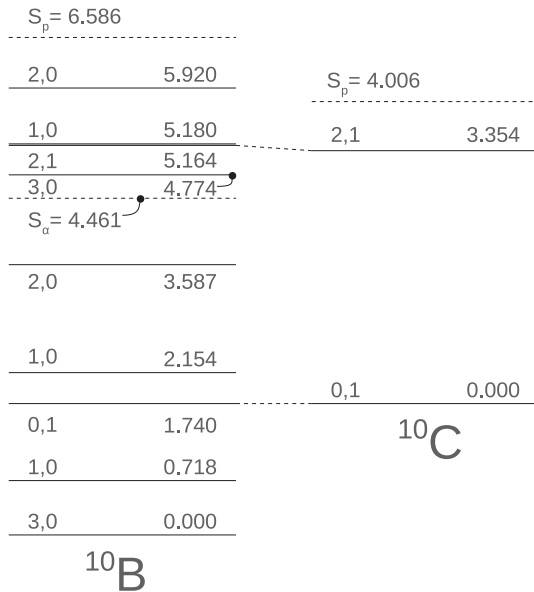


FIG. 1. States of the mass $A = 10$ residues populated in the two-nucleon removal reactions considered. The spin and isospin labels (J_f, T) are indicated. All states included are of positive parity. Levels assumed to be part of the isospin multiplet are connected by dashed lines. The lowest particle thresholds are also indicated. States above the α -particle threshold in ^{10}B are expected to decay via α emission, with the exception of the 5.164-MeV, $T = 1$, $J_f^{\pi} = 2^+$ state, which has an 84% γ -decay branch.

thus have a common theoretical input in the $T = 1$ channel. The pp -removal channel on the other hand will populate two additional $T = 1$ configurations, the 2_2^+ and 0_2^+ states. These states are particle unbound in both ^{10}B and ^{10}C and thus the pp channel has less commonality. From an experimental point of view the nn -channel predictions are also more attractive than those for pp , having (a) a very simple two-final-state spectrum and (b) a residue charge that is unchanged, meaning that the residue momentum distributions will not suffer from additional experimental broadening due to the unknown reaction point in a thick-target experiment.

In Sec. II we reiterate some specific features of the reaction description for ^{12}C projectiles. The necessary formalism, to which readers are referred, has been presented elsewhere [6,10]. We follow the notations used in these earlier works. The chiral effective field theory (EFT) two- and three-nucleon ($NN + 3N$) interactions and the microscopic NCSM calculations used to construct the improved overlap functions will be discussed in Sec. III. These include calculations in which the chiral 3N interaction is switched off in an attempt to understand the impact on observables of these 3N interaction terms in the starting Hamiltonian. The new results and predictions for ^{12}C reaction observables are analyzed in Sec. IV and a summary is presented in Sec. V.

II. CARBON-INDUCED REACTIONS

Consideration of two-nucleon removal from ^{12}C is valuable given the availability of both conventional shell-model and *ab initio* NCSM structure descriptions. The residual nuclei ^{10}C and ^{10}B (and ^{10}Be) are also extensively studied and so establish a valuable benchmark. In addition, the existing experimental cross section measurements [11,12], although inclusive with respect to the residue final states, have relatively small quoted uncertainty and were taken at high energies where the eikonal model description of the reaction dynamics is most reliable. These data were obtained for reactions of a carbon beam and carbon target at 250, 1050, and 2100 MeV per nucleon incident energies. As mentioned above, these data (and related data for other light projectile nuclei) show a significant enhancement in their $T = 0, 1$, np -removal production cross sections over those with $T = 1$, the nn - and pp -removal cases (see, e.g., Table I). This observed enhancement is of particular interest as a potential signal and a measure of strong np correlations at the nuclear surface.

The primary motivation for the present study is the implementation and first assessment of improved microscopic

descriptions of the two-nucleon overlap functions and their implications for np correlations and the calculated reaction yields and observables. The relevant final states of the $A = 10$ residual nuclei and their spins and isospins are shown in Fig. 1. The known spectrum of low-lying states in ^{10}B also contains several negative-parity states. These are not expected to be populated in the two-nucleon removal reaction mechanism. More exclusive measurements would be needed to confirm this expectation.

The isospin formalism developed in Refs. [6,10] is used here. The description of the reaction and the parameters used for the carbon target and the residue densities, etc. are the same as were discussed and tabulated in Ref. [5]. In particular the density distribution of the mass $A = 10$ residues was assumed to have a Gaussian shape with a root mean squared (rms) radius of 2.30 fm, the value quoted for ^{10}Be in Ref. [15]. In the present work the residue densities are also computed, consistent with the two-nucleon overlaps used, from the microscopic NCSM calculations that are presented. These densities, more specifically their rms radii, and their implications for the computed cross sections are discussed in Sec. IV B.

The key approximations made in Ref. [5] and this work are as follows: (a) The removal of nucleons is sudden, their coordinates being frozen during the short time scale of the relativistic, surface-grazing reactions. (b) The no-recoil (heavy residue) approximation is made [6]. The inclusion of core recoil will affect only the diffractive breakup components of the reaction mechanism. Their contributions, state by state, in the no-recoil calculations will be shown to be equal to 42(3)% of the dominant two-nucleon stripping terms, for which recoil is not an issue, and thus they contribute 30(2)% of the 2N removal cross sections. It is known from single-nucleon removal reactions, where recoil can be treated exactly, that no-recoil calculations overestimate the yield from these diffractive processes. We reiterate however that it is the fractional changes of the cross sections between the NCSM and the p -shell calculations, and between the $T = 0$ and $T = 1$ transitions, that are of most interest and significance to this work. Since the calculated fraction of the cross section due to diffractive breakup is essentially the same for all final states recoil can at most result in a common overall scaling of all of the calculated no-recoil model cross sections. We will provide an estimate of this renormalization of the diffractive terms and the removal cross sections due to recoil corrections in Sec. IV C.

The primary difference here is a now considerably extended set of two-nucleon amplitudes (TNA) C_α^{IT} arising from the multishell set of available 2N configurations $\alpha \equiv [\beta_1, \beta_2]$. Here the index $\beta = (n\ell j)$ denotes the spherical quantum numbers of each active single-particle state in the model space. We evaluate the cross sections for transitions from the projectile initial (ground) state i , with spin (J_i, M_i) , to particular residue final states f , with (J_f, M_f) . The all-important two-nucleon overlap function for removal of two nucleons 1 and 2 is

$$\Psi_i^{(F)} = \sum_{I\mu T\alpha} C_\alpha^{IT} (I\mu J_f M_f | J_i M_i) \times (T\tau T_f \tau_f | T_i \tau_i) [\overline{\psi_{\beta_1}(1)} \otimes \overline{\psi_{\beta_2}(2)}]_{I\mu}^{T\tau}. \quad (1)$$

Here $J_i^\pi = 0^+$ and thus $J_f = I$, the 2N total angular momentum. We discuss later the use of Woods-Saxon or harmonic oscillator radial functions for the single-particle orbitals ψ_β . The 2N correlations under discussion arise in Eq. (1) from (a) somewhat trivially, the antisymmetry and angular momentum coupling of nucleon pairs and (b) the possible coherent pair enhancement arising from the weights and phases of the TNA that contribute to each J_f final state. The latter and their sensitivity to (i) the NN + 3N effective interactions used and (ii) the NCSM model-space dimensions are studied here.

Importantly, unlike the earlier p -shell-only analysis, the NCSM wave functions and overlaps now include active single-particle orbitals of both parities, including up to $N_{\text{max}} = 6$ major oscillator shells. The angular correlation function of the two nucleons thus contains both even and odd Legendre polynomial terms in the angular separations of the two nucleons [13,16] with the likelihood of a greater spatial localization of pairs at the nuclear surface. The degree of such increased correlations is discussed further in the results section where we also show the two-nucleon joint-position probabilities in the impact parameter plane, $\mathcal{P}_{J_f}(s_1, s_2)$, as were defined in Ref. [13]. These display the two-nucleon spatial correlations as delivered by the projectiles and as seen by the target nucleus that induces the reaction.

Nucleon removal may occur via either elastic (diffraction) or inelastic (stripping) interactions of nucleons with the target nucleus, the former leaving the target in its ground state. The latter lead to cross section contributions that are inclusive with respect to all other target final states. Two-nucleon removal events can involve (a) both nucleons making inelastic collisions with the target, (b) there being one inelastic and one elastic collision, or (c) both nucleons suffering elastic collisions. Events (b), referred to as diffraction-stripping, are identified in the reaction's absorption cross section but require projection-off bound states for the elastically interacting nucleon (for details see Refs. [6,10]). When truncated-basis, single-major-shell, shell-model calculations have been used to generate the TNA, all active single-particle orbits in the shell were included in this projection operator. Here, when using the NCSM calculations in a very large basis, we have limited the projection to the $0p$ -shell orbitals, as being the appropriate bound states set. Purely elastic 2N-removal events (c) were estimated, as previously [6], from the stripping and diffractive-stripping cross sections. Typically, they contribute to the cross sections at the level of <5%.

The absorptive eikonal S matrices, which largely determine the volume of the two-nucleon overlap function that is sampled in the reaction, were calculated by folding the target, nucleon, and reaction residue point-nucleon densities with a zero-range effective nucleon-nucleon interaction. Further details may be found in Ref. [5]. Our primary interest is in the np -removal cross sections. Since both the 0_1^+ and 2_1^+ $T = 1$ states are populated in both ^{10}B and ^{10}C we also discuss the cross section for the nn channel. Only very minor differences in these partial cross sections will arise from (a) the use of a ^{10}B rather than a ^{10}C S matrix and (b) the small binding energy differences. Unlike the earlier p -shell calculations, which used Woods-Saxon single-particle wave functions, the latter are not

accounted for in the present calculations that use harmonic oscillator radial wave functions.

III. NN + 3N INTERACTIONS AND OVERLAPS

The p -shell ($0\hbar\omega$) shell-model calculations and overlaps were described in Ref. [5] and were computed using the code OXBASH [17]. For the present work, a series of no-core-shell-model calculations, each for a given number of major oscillator shells, $N_{\max} = 0, 2, 4, \text{ or } 6$, were carried out using two chiral EFT NN + 3N interaction choices, denoted NCSM1 and NCSM2 in the following.

The calculations used interactions derived within the chiral EFT approach. In particular, the chiral next-to-next-to-next-to-leading order ($N^3\text{LO}$) NN interaction of Refs. [18,19] was used with or without the chiral next-to-next-to-leading order ($N^2\text{LO}$) 3N interaction [20] in the local form of Ref. [21]. These interactions were softened by the similarity renormalization group (SRG) technique [22–24], where a unitary transformation is used to suppress the off-diagonal matrix elements (controlled by a parameter Λ). The SRG interaction induces higher-body interaction terms. These induced terms were kept up to the three-body level. It has been shown [25,26] that four- and higher-body terms are negligible for light nuclei although some evidence for four-body-induced terms was observed in ^{12}C calculations with one of the interactions used here (NCSM2) [26]. In NCSM1 the NN + 3N Hamiltonian used a 3N cutoff of 400 MeV and used parameters fitted to the ^3H lifetime and the ^4He binding energy [27]. In NCSM2 the 3N cutoff was 500 MeV and the parameters were fitted to the lifetime and binding energy of ^3H [28]. For both NCSM1 and NCSM2 the SRG was carried out using $\Lambda = 1.7 \text{ fm}^{-1}$ and $\Lambda = 1.88 \text{ fm}^{-1}$ to verify the SRG Λ independence, i.e., to confirm the unitarity of the SRG transformation. The subsequent NCSM calculations used a harmonic oscillator (HO) basis with an angular frequency $\hbar\omega = 16 \text{ MeV}$. The mass-dependent parametrizations of the oscillator frequency, agreeing with charge radius observations, suggest a value of $\hbar\omega = 14.9 \text{ MeV}$ [29], in reasonable agreement with the value used here.

In the case of the NCSM2 parametrization, the calculations were also repeated, and denoted as NCSM3, with the chiral 3N interaction in the starting Hamiltonian switched off, but with the SRG-induced 3N effects (with $\Lambda = 1.7 \text{ fm}^{-1}$) included. Again, the HO frequency of $\hbar\omega = 16 \text{ MeV}$ was employed. Using these NCSM3 TNA we can make a first assessment of the impact on calculations and observables of the inclusion, or not, of the chiral 3N interaction in the starting Hamiltonian.

It should be noted that the ^{10}B structure poses a particular challenge to *ab initio* calculations. In particular, it had been observed that standard accurate NN potentials predict incorrectly the ground state of ^{10}B to be 1^+0 , instead of the experimental 3^+0 . The present calculations with the chiral $N^3\text{LO}$ NN potential (NCSM3) suffer from the same problem. Only after including the chiral $N^2\text{LO}$ 3N term, with the 3N cutoff of 500 MeV, NCSM2, does one get the correct ground-state spin. Interestingly, the weaker chiral $N^2\text{LO}$ 3N with the 3N cutoff 400 MeV, NCSM1, fails to invert the 1^+0

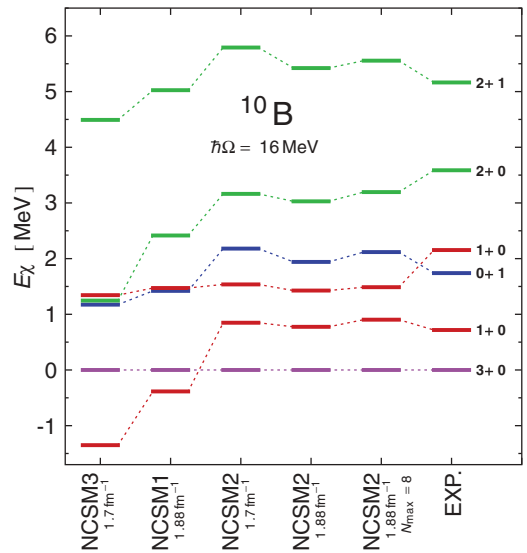


FIG. 2. (Color online) Experimental excitation energies of ^{10}B compared to the different calculations used in the present work: chiral $N^3\text{LO}$ NN (NCSM3), chiral $N^3\text{LO}$ NN plus $N^2\text{LO}$ 3N with the cutoff of 400 MeV (NCSM1), and chiral $N^3\text{LO}$ NN plus $N^2\text{LO}$ 3N with the cutoff of 500 MeV (NCSM2). The $N_{\max} = 6$ space was used in calculations shown in the first four columns. The SRG Λ parameter is indicated. The HO frequency of $\hbar\omega = 16 \text{ MeV}$ was used in all calculations.

and 3^+0 states, also predicting the wrong ^{10}B ground-state spin. See Fig. 2 for a comparison of ^{10}B excitation energies from different calculations used in this paper. Also in the figure, the stability of the spectra with respect to the SRG Λ variation and the size of the model space, N_{\max} , is demonstrated for the NCSM2 case. The situation is somewhat reversed in ^{12}C , where the Hamiltonian NCSM2 with the stronger 3N interaction overbinds ^{12}C by several MeV and overcorrects the splitting of the 1^+0 and 4^+0 states [26]. Using the weaker 3N interaction (NCSM1) improves both the binding energy and excitation energy description. Furthermore, this Hamiltonian (NCSM1) also describes the binding energies of oxygen and calcium isotopes [27] very well. The stronger 3N interaction NCSM2, on the other hand, provides a very good description of lighter nuclei ($A \leq 10$), resolving even long-standing analyzing power problems in p - ^3He scattering [30]. These observations suggest that our knowledge of the 3N interaction in particular is incomplete and additional terms, such as those at the $N^3\text{LO}$ of chiral perturbation theory, must be included. Further, the mass region of $A = 10$ –12 is ideal to test the details of the nuclear Hamiltonians.

IV. RESULTS

A. Reaction calculations

Reaction calculations were carried out using the extended two-nucleon-amplitude sets derived from the effective interactions outlined in Sec. III, for each of $N_{\max} = 0, 2, 4, \text{ and } 6$ and for the nn - and np -removal channels. We present calculations for NCSM1 ($\Lambda = 1.88 \text{ fm}^{-1}$) and NCSM2

TABLE II. Calculated inclusive cross sections for two-nucleon removals from ^{12}C , for projectile energies of 250, 1050, and 2100 MeV per nucleon. All cross sections are in millibarns. The TNA used were calculated using the $0p$ -shell and WBP interaction and the NCSM1 and NCSM2 NN + 3N interactions with $N_{\text{max}} = 6$. The experimental cross sections were given in Table I.

Energy (MeV/u)	^{10}C			^{10}B		
	$\sigma_{-2n}^{\text{WBP}}$	$\sigma_{-2n}^{\text{NCSM1}}$	$\sigma_{-2n}^{\text{NCSM2}}$	$\sigma_{-np}^{\text{WBP}}$	$\sigma_{-np}^{\text{NCSM1}}$	$\sigma_{-np}^{\text{NCSM2}}$
250	5.93	7.10	8.48	21.20	28.19	29.91
1050	5.22	6.31	7.44	18.71	25.26	26.45
2100	5.12	6.22	7.28	18.36	25.00	26.01

and NCSM3 ($\Lambda = 1.7 \text{ fm}^{-1}$). In Table II we first show the calculated inclusive cross sections for the (most complete) NCSM $N_{\text{max}} = 6$ calculations at the three energies of the available data. We also compare to results using $0p$ -shell WBP shell-model TNA. All calculations use harmonic oscillator radial form factors with $\hbar\omega = 16 \text{ MeV}$, as used in the NCSM basis. We note that the previous $0p$ -shell WBP calculations of Ref. [5] used Woods-Saxon radial wave functions when constructing the two-nucleon overlap functions. The use of fixed $\hbar\omega = 16 \text{ MeV}$ oscillator functions introduces small excitation-energy-dependent changes to the cross sections, due to the absence of any binding energy effect. For the lowest energy 3^+ state, the cross section is reduced by $\sim 7\%$. This reduction becomes progressively smaller as the state excitation increases, with the cross sections to the highest energy states slightly enhanced.

Here we consider only the WBP shell-model interaction; calculations using the PJT and WBP interactions give consistent final-state-inclusive cross sections. When using the PJT $0p$ -shell effective interaction (with Woods-Saxon form factors as per Ref. [5]) the inclusive ^{10}B yield at 2.1 GeV per nucleon was 18.73 mb, as compared to 19.02 mb for the WBP case shown in Table I. Further details and the comparison between these calculations can be found in Ref. [5].

The cross sections, now exclusive with respect to the $A = 10$ final states, are shown in Table III for the highest energy of 2.1 GeV per nucleon. The two NN + 3N NCSM cases (with $N_{\text{max}} = 6$) and the WBP case are shown together with the NCSM3 case (i.e., without the chiral 3N interaction in the starting Hamiltonian). In np removal to ^{10}B the cross sections are shown for the six positive-parity γ -decaying final states below the first nucleon threshold. However, the first 2^+ , $T = 1$ state is known to decay by α emission with an $I_\alpha = 16\%$ branch. This branching has been accounted for in the inclusive σ_{-2N} values presented. The cross sections for population of the three higher-lying $T = 0$ states (see Fig. 1) are not included since these states are reported to decay by α emission (with $I_\alpha = 100\%$). It was assumed that these states do not contribute to the ^{10}B yields.

Table III reveals significant sensitivity of the yields of the low-lying ^{10}B states to the interactions assumed. The ratio of the $T = 0$, 1_1^+ to 3^+ ground-state yields is reversed between NCSM1 and NCSM2. The absence of the 3N interaction in the NCSM2 starting Hamiltonian, the NCSM3 case, leads to

TABLE III. Like and unlike two-nucleon removal cross sections (in millibarns) for a ^{12}C projectile incident on a carbon target at 2100 MeV per nucleon. The excitation energies, E_f , of each final state are shown in Fig. 1. The TNA used were calculated using (a) the $0\hbar\omega$ p -shell-model and WBP interaction, (b) the two NN + 3N interactions NCSM1 and NCSM2 (see text), and (c) the NCSM3 Hamiltonian in which the chiral 3N interaction is turned off. Calculations (b) and (c) use the NCSM with $N_{\text{max}} = 6$. The sums show the accumulated cross sections that lead to the ground state and the γ -decaying bound excited states of the mass $A = 10$ projectile residues.

Residue	J_f^π	T	$\sigma_{-2N}^{\text{WBP}}$	$\sigma_{-2N}^{\text{NCSM1}}$	$\sigma_{-2N}^{\text{NCSM2}}$	$\sigma_{-2N}^{\text{NCSM3}}$
^{10}C	0^+	1	2.29	3.93	3.67	4.11
	2^+	1	2.83	2.29	3.61	2.27
Inclusive			5.12	6.22	7.28	6.38
Experiment				4.11 ± 0.22		
^{10}B	3^+	0	6.78	7.56	9.32	6.11
	1^+	0	3.48	8.52	7.22	10.18
	0^+	1	2.29	3.93	3.67	4.11
	1^+	0	2.51	1.93	1.60	2.13
	2^+	0	0.92	1.13	1.17	1.22
	2^{+a}	1	2.38	1.92	3.03	1.91
Inclusive			18.36	25.00	26.01	25.66
Experiment				35.10 ± 3.40		

^aState decays by α emission with a 16% α branch.

a quite significantly enhanced ratio of the $T = 0$, 1_1^+ to 3^+ ground-state cross sections when compared to the full NCSM2 Hamiltonian. To confront these detailed model predictions requires more exclusive measurements with good statistics.

The six contributing ^{10}B partial cross sections are also plotted in Figs. 3, 4, 5, and 6. Figure 3 shows the calculations, using NCSM1, for $N_{\text{max}} = 0, 2, 4$, and 6, and the stabilization and the essential convergence of the calculated partial cross sections (upper panel) and the full width at half-maximum widths of their momentum distributions (lower panel) with increasing N_{max} . Based on this observed convergence, seen for all of the NCSM cases, we have presented, in the main, only the final $N_{\text{max}} = 6$ results. Figure 4 shows $N_{\text{max}} = 6$ NCSM2 calculations for two different SRG Λ values, $\Lambda = 1.7 \text{ fm}^{-1}$ and $\Lambda = 1.88 \text{ fm}^{-1}$. The essential independence of the cross sections and the FWHM on the SRG Λ values confirms the unitarity of the SRG transformation; i.e., we are really investigating predictions of the initial chiral interactions. Based on the results of Ref. [26], the SRG Λ dependence is expected to be even weaker for the NCSM1 and NCSM3 cases. Figure 5 shows the calculations from the NCSM1, NCSM2, and NCSM3 Hamiltonians, all with $N_{\text{max}} = 6$. The significant variations predicted in the widths of the momentum distributions for the different final states and the sensitivity of the $T = 0$, ^{10}B final-state yields to these effective interactions are evident. The momentum distribution widths from the NCSM interactions are broadly consistent and are also consistent with those of the conventional truncated-basis p -shell model interactions (shown in Fig. 6). These similarities reflect the relative insensitivity of the different LS fractions in the overlap to the interactions used. The notable exception is the second $T = 0$, 1^+ excited state, when the width using the NCSM interactions

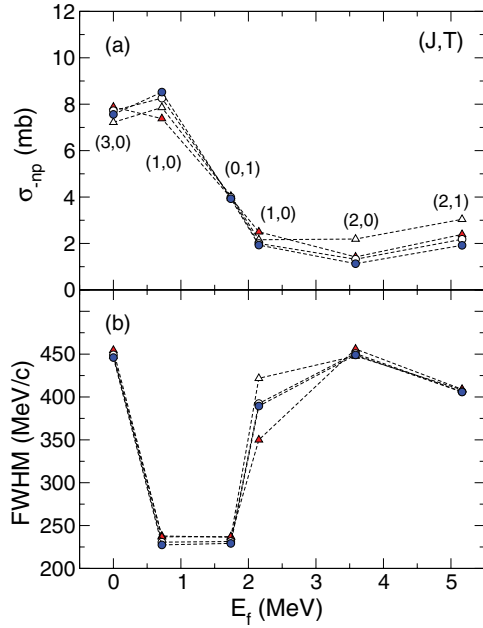


FIG. 3. (Color online) (a) Calculated exclusive cross sections and (b) full width at half maximum (FWHM) widths of the momentum distributions for the ground and γ -decaying final states of the ^{10}B residues, following np removal at 2100 MeV per nucleon. The TNA used were obtained using the NCSM1 NN + 3N starting Hamiltonian with SRG $\Lambda = 1.88 \text{ fm}^{-1}$ (dashed lines). Calculations are for $N_{\max} = 0$ (open triangles), 2 (red triangles), 4 (open circles), and 6 (blue circles).

is somewhat wider than that from the conventional shell-model interactions. More generally, some systematic differences with calculations of Ref. [5] are found; the present calculations are wider by $\approx 25 \text{ MeV}/c$. We attribute this to the incorrect asymptotic of the oscillator wave functions.

The final-state-inclusive cross sections for the NCSM interactions are all larger than those from the truncated-space WBP interaction. All three NCSM interactions result in similar summed cross sections to the lowest two $T = 0$ states, between 16 and 17 mb, but the distribution of this strength between the two states shows significant variations. The cross sections to the $T = 1, 0^+$ state are also larger when using the NCSM interactions with variations between the predictions of the interactions, reinforcing the need for final-state-exclusive cross-section measurements. The detailed nature of the sensitivity of the TNA, and hence the final-state branching ratios and cross sections, to the details of the interactions is complex, but precise measurements could provide a path to probe this sensitivity and toward constraining the underlying interactions.

The ratios of the theoretical model and experimental cross sections, $R_s(2N) = \sigma_{\text{exp}}/\sigma_{\text{th}}$, are $R_s(2n) = 0.66$ and $R_s(np) = 1.40$ for the NCSM1 interaction and $R_s(2n) = 0.56$ and $R_s(np) = 1.35$ for NCSM2. Calculations for two-nucleon removal in exotic sd -shell isotopes typically overestimate the experimental observations by a factor of 2 with $R_s(2N) = 0.5$ [6]. As mentioned above, we do not include core recoil and center-of-mass effects for the structure amplitudes, but these effects will affect the np and nn channels similarly. We discuss

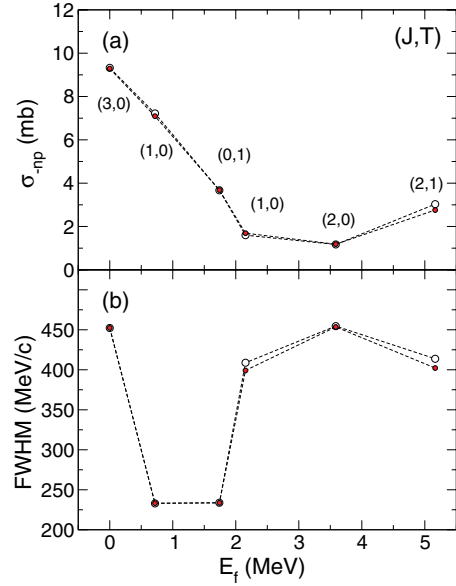


FIG. 4. (Color online) (a) Calculated exclusive cross sections and (b) FWHM widths of the momentum distributions for the ground and γ -decaying final states of the ^{10}B residues, following np removal at 2100 MeV per nucleon. The TNA used were obtained using the NCSM2 NN + 3N starting Hamiltonian (dashed lines). Calculations are for $N_{\max} = 6$ with the SRG $\Lambda = 1.7 \text{ fm}^{-1}$ (open circles) and $\Lambda = 1.88 \text{ fm}^{-1}$ (red circles).

the effects of recoil and its implications for the absolute cross sections [and hence $R_s(2N)$] further in Sec. IV C.

To consider the impact of the significantly larger model spaces introduced using the NCSM amplitudes, it is meaningful to consider the cross-section ratios $\sigma_{-2N}^{\text{WBP}}/\sigma_{-2N}^{\text{NCSM}}$, i.e., the relative enhancement of a particular channel when moving from the truncated-basis WBP to the NCSM interactions. For the NCSM1 interaction, this ratio is 0.82 for the nn channel and 0.73 for the np channel. The corresponding ratios for the NCSM2 interaction are 0.70 and 0.71, respectively. Evidently, the use of the larger-basis-amplitude set enhances the cross section.

A significant component of these differences results from changes in the p -shell amplitudes, as are shown in Table IV, the simplest case being the 3^+ ground state, where only a single p -shell configuration contributes. The $[0p_{3/2}]^2$ TNA vary, depending on the different interactions, and the magnitude of these p -shell amplitudes is a key factor in the cross-section changes observed. For the two $T = 0, 1^+$ states, a mix of p -shell configurations now contribute, with the overall magnitude of the TNA and their relative strengths and phases changing. The relative strengths of the three configurations are broadly consistent across the NCSM interactions, but they are different from the truncated-basis WBP interaction. In particular the $[p_{3/2}]^2$ TNA are different, with some apparent shift of strength from the first to the second 1^+ state, when compared to the NCSM interactions. In these cases there is interference between the different configurations that makes what one expects from the different interactions less transparent. Changes in the p -shell configurations will account for a part of the changes in cross sections shown in Table III and

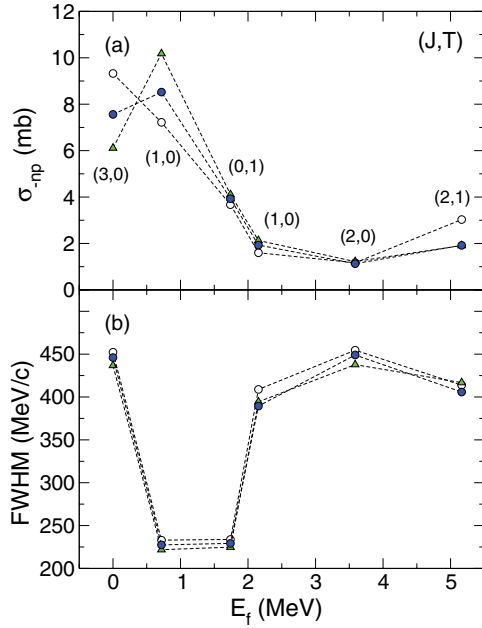


FIG. 5. (Color online) (a) Calculated exclusive cross sections and (b) FWHM widths of the momentum distributions for the ground and γ -decaying final states of the ^{10}B residues, following np removal at 2100 MeV per nucleon. The TNA used were obtained using the NCSM1 (blue circles) and NCSM2 (open circles) NN + 3N starting Hamiltonians and the NCSM3 (green triangles) NN starting Hamiltonian, all for $N_{\text{max}} = 6$.

the predicted momentum distribution widths for the second 1^+ state, offering a means to discern between the different interactions.

Further enhancement of the cross section may arise from the new couplings to higher major shells. Coupling to major shells of the same parity (odd N) will lead to generic changes to the overall size of the two-nucleon overlap functions and TNA. The TNA due to mixing with major shells of opposite parity (even N) lead to new interference effects that can enhance two-nucleon spatial correlations (see, e.g., [16]). For the first 1^+ this can be seen in Fig. 7 for calculations based on the NCSM1 Hamiltonian. The left panel is calculated when retaining only the $0\hbar\omega$ p -shell two-nucleon-amplitude components from the $N_{\text{max}} = 6$ NCSM calculation. The right panel includes the full set of NCSM TNA for all major shells. The enhanced spatial correlations presented to the target nucleus from the inclusion of single-particle configurations with opposite parity in the two-nucleon overlap function are evident. The cross sections from these truncated and full sets of TNA are 6.09 and 8.52 mb, respectively. Both exceed those of the p -shell shell-model calculations, this being 3.48 mb for the WBP interaction TNA.

For the NCSM1 interaction the enhancement of the np -removal cross sections relative to the WBP calculations is larger than that for the like-nucleon-removal (nn -removal) cross section, whereas the calculations with NCSM2 show no significant relative enhancement. Despite the larger np -removal cross section obtained, the experimental np -channel cross sections continue to be underestimated. The available

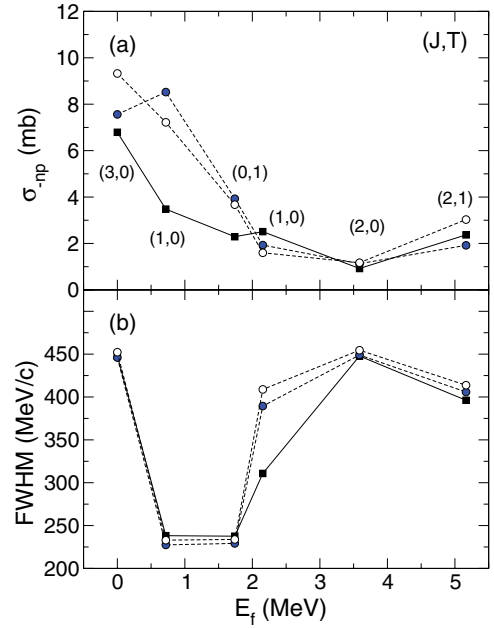


FIG. 6. (Color online) (a) Calculated exclusive cross sections and (b) FWHM widths of the momentum distributions for the ground and γ -decaying final states of the ^{10}B residues, following np removal at 2100 MeV per nucleon. The TNA used were obtained using the WBP shell-model interaction (solid lines and solid squares) and the NCSM1 (dashed lines and blue circles) and NCSM2 (dashed lines and open circles) NN + 3N Hamiltonians for $N_{\text{max}} = 6$.

data again suggest that there are remaining deficiencies in the $T = 0$ parts of the two-nucleon overlap functions due to the relative discrepancy between nn and np channels. The yields to specific final states, namely, the first 3^+ , 1^+ , and 0^+ states, suggest a significant sensitivity to the interactions used, requiring input from final-state-exclusive measurements.

B. Core density effects

As was stated in Sec. II, the calculations of the previous section made use of residue-target S matrices computed using a fixed (Gaussian) single-particle density for the mass 10

TABLE IV. $0p$ -shell two-nucleon amplitudes for the WBP, NCSM1, NCSM2, and NCSM3 interactions with $N_{\text{max}} = 6$.

Interaction	(J^π, T)	$[p_{1/2}]^2$	$[p_{1/2}][p_{3/2}]$	$[p_{3/2}]^2$
WBP	$(3_1^+, 0)$	–	–	1.976
	$(1_1^+, 0)$	–0.011	0.979	0.699
	$(1_2^+, 0)$	0.363	0.229	–1.134
NCSM1	$(3_1^+, 0)$	–	–	1.913
	$(1_1^+, 0)$	–0.220	1.034	1.197
	$(1_2^+, 0)$	0.611	0.376	–0.835
NCSM2	$(3_1^+, 0)$	–	–	2.213
	$(1_1^+, 0)$	–0.255	0.863	1.307
	$(1_2^+, 0)$	0.470	0.500	–0.814
NCSM3	$(3_1^+, 0)$	–	–	1.644
	$(1_1^+, 0)$	–0.224	1.137	1.205
	$(1_2^+, 0)$	0.740	0.332	–0.719

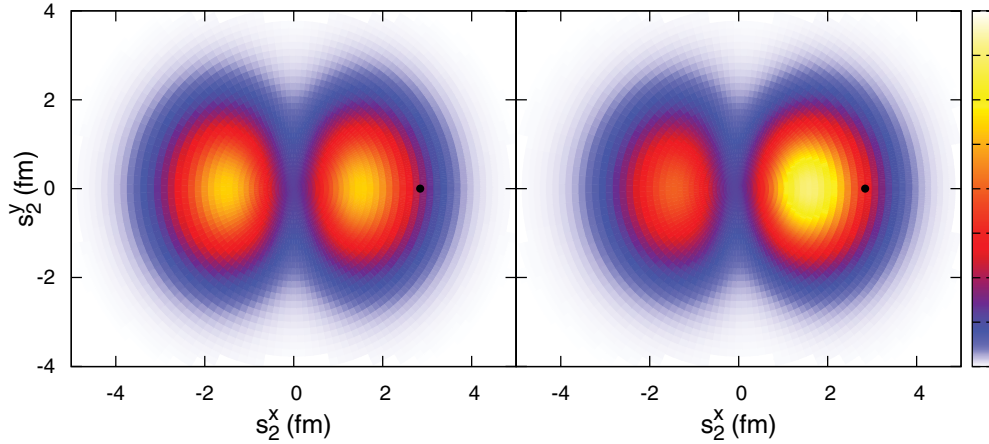


FIG. 7. (Color online) Projected two-nucleon density $\mathcal{P}_f(s_1, s_2)$ from the two-nucleon overlap for the first $T = 0, 1^+$ state, calculated using the NCSM and the NCSM1 Hamiltonian. The contours show the position probability in the impact parameter plane of nucleon 2, s_2 , when nucleon 1, s_1 , is at the position indicated by the black point. The left panel is calculated when retaining only the lowest p -shell TNA from the $N_{\max} = 6$ calculation. The right panel includes the full set of NCSM TNA for $N_{\max} = 6$. The overlap shows the enhanced spatial correlations arising from inclusion of single-particle configurations of opposite parity in the two-nucleon overlap function (see also Fig. 4 of Ref. [13]). The cross sections from these two sets of TNA are 6.09 and 8.52 mb, respectively.

residues with rms radius $R_0 = 2.30$ fm. As a result of the strong absorption of the deduced residue-target interactions and S matrices the calculated cross sections are insensitive to any details of the density distribution other than its rms radius, R_c , which dictates the range of the absorption and hence the reaction geometry. The 2N-removal cross-section calculations, being surface localized, scale essentially linearly with small changes in R_c . For the present $^{12}\text{C}(-2\text{N})$ transitions we compute this dependence to be

$$\sigma(R_c) = \sigma(R_0)(1 - 1.1 \delta R_c),$$

with $\delta R_c = R_c - R_0$ the deviation of the rms radius from the chosen value.

The NCSM calculations presented also compute these residue R_c values microscopically for each interaction and N_{\max} , consistent with the overlap functions and the TNA used. The residue densities for each interaction show small individual deviations from our fixed R_c value, introducing a small error on the deduced cross sections, quantified based on the differential δR_c sensitivity shown above. For the most complete $N_{\max} = 6$ calculations the mean computed R_c values for the 3^+ and 1^+ final states are 2.292, 2.256, and 2.371 fm in the NCSM1, NCSM2 and NCSM3 cases, respectively. Thus the associated effects on our tabulated cross sections are of order -1.0% , -4.4% , and $+7.8\%$ for the three interactions used. Such finer differences and details can and should be included in the quantitative analysis of future final-state-exclusive measurements.

C. Recoil effects

The calculations presented here make the no-recoil approximation in which it is assumed that the projectile core position is coincident with the projectile center of mass. We now discuss and estimate the degree to which this approximation may

overestimate the diffraction-stripping cross sections in these relatively light residue reactions; the dominant two-nucleon stripping mechanism will be unaffected. For two-proton knockout from ^{28}Mg , calculations using the present no-recoil approach reproduce the relative strengths of stripping and diffraction-stripping mechanisms within experimental errors [7]; the experimental and theoretical diffraction-stripping branching ratios were found to be $b_{\text{exp}} = 31(16)\%$ and $b_{\text{th}} = 37.4\%$. Here, the recoil corrections for the light ^{12}C projectile will be considerably larger. We reiterate that, since the calculated fraction of the cross section due to the diffraction-stripping mechanism is, to an excellent approximation, the same for all transitions [30(2)%], the recoil corrections will result only in a common overall scaling of all of the calculated no-recoil model cross sections that are presented above.

Guidance on the importance of recoil effects can be obtained from single-nucleon removal calculations where recoil is treated exactly. Eikonal model calculations similar to those presented here accurately reproduce the fraction of elastic-breakup events for knockout from light systems when core recoil is included ($^9\text{C}(-1\text{p})$ and $^8\text{B}(-1\text{p})$ [31]). For the current systems, i.e., $^{12}\text{C}(-1\text{N})$ nucleon removal, the full-recoil calculations reduce the diffractive cross-section components to 0.65(3) of their no-recoil values. Geometrically, the dominant spatial configurations for these removal reactions are those where a nucleon is closest to the target, with small impact parameters b_v , and so can interact strongly, and the core nucleons are distant from the target, with larger impact parameter b_c , and so undergo at most elastic interactions. The above reduction is thus expected since with no recoil one assumes the core (residue) impact parameter coincides with that of the projectile center of mass, $b = b_c$, which forces the nucleon closer to the target in the most important spatial configurations for nucleon removal. This geometrical picture also suggests that the dominant effects of recoil might be included approximately by changing the impact parameters

at which the nucleon-target S matrix is evaluated: specifically, by replacing $b_v \rightarrow b_v + r/12$, where r is the nucleon-core separation distance, which is of the order the projectile radius for the removal of well-bound nucleons of interest here. Calculations for a number of single-nucleon removal transitions in which this nucleon impact parameter correction was made in an otherwise no-recoil calculation were found to reproduce the diffractive cross sections from the full-recoil calculations to within 10% in all cases.

The analogous correction for two-nucleon removal ($i = 1, 2$) would be $b_i \rightarrow b_i + r/6$. This might account for (a) the reaction mechanism needing to find two nucleons in near proximity at the nuclear surface and (b) the favored geometry for the majority of 2N-removal events. We have applied this impact parameter correction for a number of transitions to the two-nucleon cases above. The diffraction-stripping cross sections, which in the no-recoil calculations above are 42(3)% of the calculated stripping cross sections, and thus 30(2)% of the total 2N-removal cross sections, were found to be substantially reduced. With the approximate recoil correction these are 13(1)% of the corresponding stripping terms and thus only of order 11(1)% of the calculated 2N-removal yields.

So, based on these estimates the no-recoil calculations of Sec. IV A will overestimate the diffraction-stripping components and should all be scaled by a common factor. We place a significant additional uncertainty (of 30%) on these simple diffraction-stripping cross-section estimates and the deduced scaling factor is thus $1.13(4)/1.42 = 0.80(3)$. The relative magnitudes of all cross sections are unchanged. We emphasize that this is an approximate first estimate of recoil effects on the diffraction-stripping cross section, but the suggested magnitude of these effects clearly motivates the full inclusion of recoil as being important to quantify the absolute cross sections for these lighter systems. A calculation of these absolute cross sections was not the primary aim here.

V. SUMMARY

We have considered the impact of microscopic NCSM wave function overlaps on the theoretical cross sections for two-nucleon removal reactions from fast ^{12}C projectiles. Data were available for reactions on a carbon target at beam energies of 250, 1050, and 2100 MeV per nucleon. As found in a previous analysis [5], the np -removal cross sections are

underestimated by the theoretical model calculations, but they do show an enhancement relative to the use of truncated-basis p -shell-model calculations. The cross sections to both $T = 0$ and $T = 1$ states are enhanced, and the use of large-basis NCSM amplitudes does not fully resolve the relative discrepancy between measured np - and nn -removal cross sections.

Further measurements, of final-state-exclusive cross sections and residue momentum distributions, would allow for a much more detailed scrutiny and confrontation of the predictions from detailed reaction observables, including the identification of any indirect reaction components arising from two-step paths to the final states. The calculated np -removal cross sections to the $T = 0$, ^{10}B final states were shown to have sensitivity to the different variants of the chiral interactions used, for example, the ratio of the calculated cross sections to the ^{10}B ground 3^+ , $T = 0$ and first 1^+ , $T = 0$ excited states. To a lesser degree the first 0^+ , $T = 1$ state cross section and the branching between the first $T = 1$, 0^+ and 2^+ states was found to depend on the effective interaction. In this case, data for the nn - and pp -removal channels would provide useful verification. The momentum distribution of the second 1^+ , $T = 0$ state also shows a particular sensitivity to the interaction, providing a further useful probe.

The overall conclusion from the present analysis is that the existing residue-final-state-inclusive data suggest that the $T = 0$, np -spatial correlations present in the wave functions used are still insufficient. We have shown that new exclusive measurements would offer a means to interrogate these shell-model inputs, in particular for the np -channel, $T = 0$ wave functions, and the direct reaction mechanism predictions in considerable detail. Additionally, we show that a full-recoil treatment will be needed to precisely establish the diffraction-stripping contributions and absolute two-nucleon removal cross sections for these lighter systems with $A \leq 12$.

ACKNOWLEDGMENTS

This work was supported by the United Kingdom Science and Technology Facilities Council (STFC) under Grant No. ST/J000051/1 and by NSERC Grant No. 401945-2011. Computing support for this work came in part from the LLNL institutional Computing Grand Challenge program. Partly supported by the DFG through SFB 634 and by HIC for FAIR.

-
- [1] P. G. Hansen and J. A. Tostevin, *Annu. Rev. Nucl. Part. Sci.* **53**, 219 (2003).
 [2] B. A. Brown, P. G. Hansen, B. M. Sherrill, and J. A. Tostevin, *Phys. Rev. C* **65**, 061601 (2002).
 [3] J. R. Terry, D. Bazin, B. A. Brown, J. Enders, T. Glasmacher, P. G. Hansen, B. M. Sherrill, and J. A. Tostevin, *Phys. Rev. C* **69**, 054306 (2004).
 [4] K. Wimmer *et al.*, *Phys. Rev. Lett.* **109**, 202505 (2012).
 [5] E. C. Simpson and J. A. Tostevin, *Phys. Rev. C* **83**, 014605 (2011).
 [6] J. A. Tostevin and B. A. Brown, *Phys. Rev. C* **74**, 064604 (2006).
 [7] K. Wimmer *et al.*, *Phys. Rev. C* **85**, 051603(R) (2012).

- [8] E. K. Warburton and B. A. Brown, *Phys. Rev. C* **46**, 923 (1992).
 [9] R. E. Julies, W. A. Richter, and B. A. Brown, *South African J. Phys.* **15**, 35 (1992).
 [10] E. C. Simpson, J. A. Tostevin, D. Bazin, B. A. Brown, and A. Gade, *Phys. Rev. Lett.* **102**, 132502 (2009); E. C. Simpson, J. A. Tostevin, D. Bazin, and A. Gade, *Phys. Rev. C* **79**, 064621 (2009).
 [11] J. M. Kidd, P. J. Lindstrom, H. J. Crawford, and G. Woods, *Phys. Rev. C* **37**, 2613 (1988).
 [12] P. J. Lindstrom, D. E. Greiner, H. H. Heckman, Bruce Cork, and F. S. Bieser, LBL Report No. LBL3650, 1975 (unpublished); also tabulated in D. L. Olson, B. L. Berman, D. E. Greiner,

- H. H. Heckman, P. J. Lindstrom, and H. J. Crawford, *Phys. Rev. C* **28**, 1602 (1983).
- [13] E. C. Simpson and J. A. Tostevin, *Phys. Rev. C* **82**, 044616 (2010).
- [14] J. A. Tostevin, G. Podolyák, B. A. Brown, and P. G. Hansen, *Phys. Rev. C* **70**, 064602 (2004).
- [15] A. Ozawa *et al.*, *Nucl. Phys. A* **693**, 32 (2001).
- [16] W. T. Pinkston, *Phys. Rev. C* **29**, 1123 (1984).
- [17] B. A. Brown *et al.*, OXBASH for Windows, MSU-NSCL Report No. 1289, 2004.
- [18] D. R. Entem and R. Machleidt, *Phys. Rev. C* **68**, 041001 (2003).
- [19] R. Machleidt and D. R. Entem, *Phys. Rep.* **503**, 1 (2011).
- [20] E. Epelbaum, A. Nogga, W. Glockle, H. Kamada, U.-G. Meissner, and H. Witala, *Phys. Rev. C* **66**, 064001 (2002).
- [21] P. Navratil, *Few-Body Syst.* **41**, 117 (2007).
- [22] S. D. Glazek and K. G. Wilson, *Phys. Rev. D* **48**, 5863 (1993).
- [23] F. Wegner, *Ann. Phys. (Leipzig)* **506**, 77 (1994).
- [24] E. D. Jurgenson, P. Navratil, and R. J. Furnstahl, *Phys. Rev. Lett.* **103**, 082501 (2009).
- [25] E. D. Jurgenson, P. Navratil, and R. J. Furnstahl, *Phys. Rev. C* **83**, 034301 (2011).
- [26] R. Roth, J. Langhammer, A. Calci, S. Binder, and P. Navratil, *Phys. Rev. Lett.* **107**, 072501 (2011).
- [27] R. Roth, S. Binder, K. Vobig, A. Calci, J. Langhammer, and P. Navratil, *Phys. Rev. Lett.* **109**, 052501 (2012).
- [28] D. Gazit, S. Quaglioni, and P. Navratil, *Phys. Rev. Lett.* **103**, 102502 (2009).
- [29] J. Blomqvist and A. Molinari, *Nucl. Phys. A* **106**, 545 (1968).
- [30] M. Viviani, L. Girlanda, A. Kievsky, L. E. Marcucci, and S. Rosati, *EPJ Web of Conferences* **3**, 05011 (2010).
- [31] D. Bazin *et al.*, *Phys. Rev. Lett.* **102**, 232501 (2009).